Aerodynamic Design of Blended Wing-Body and Lifting-Fuselage Aircraft

Thomas A. Reist* and David W. Zingg†

Institute for Aerospace Studies, University of Toronto

4925 Dufferin St., Toronto, Ontario, M3H 5T6, Canada

High-fidelity aerodynamic shape optimization based on the Reynolds-averaged Navier-Stokes equations is used to optimize the aerodynamic performance of conventional and blended wing-body (BWB) aircraft for a range of aircraft sizes from regional to wide-body classes. Trim-constrained drag minimization is performed, with optimized conventional tube-and-wing (CTW) designs serving as performance references. First, a set of 'classically' shaped BWB configurations are optimized across the range of classes. The classically shaped regional and narrow-body-class BWBs offer only a marginal fuel-burn benefit relative to the equivalent conventional designs. The wide-body-class BWB offers up to 10.9% lower fuel-burn than the equivalent CTW. Exploratory optimizations with significant geometric freedom are then performed, resulting in a set of novel shapes with a more slender lifting fuselage and distinct wings. Based on these exploratory results, new lifting-fuselage configurations (LFCs) are designed. The slenderness of the LFC fuselage decreases with aircraft size, such that, for the largest class, the LFC reduces to a classical BWB shape. Due to their lower weight and higher aerodynamic efficiency, the LFC designs burn 6.1% and 9.7% less fuel in cruise than the equivalent CTWs for the regional and narrow-body classes, respectively. In addition, the LFCs are more aerodynamically efficient and burn less fuel than the BWBs. Additional optimizations were performed to determine the aerodynamically optimal cruise altitude of all of the aircraft. Due to their lower wing loading, the resulting increase in cruise altitude is most beneficial for the BWBs, such that the regional and narrow-body-class BWBs burn up to 5.5% less fuel than the CTWs. The LFCs offer up to a 10.3% fuel-burn reduction relative to the CTWs when at their optimal altitude.

Nomenclature

CTW	Conventional tube-and-wing
BWB	Blended wing-body
LFC	Lifting-fuselage configuration
PAX	Passengers
MAC	Mean aerodynamic chord
b	Total aircraft span
S	Reference planform area
AR_{wet}	Wetted aspect ratio ($AR_{\text{wet}} = b^2/S_{\text{wet}}$)
V	Volume
q_∞	Freestream dynamic pressure
L, D, M	Total lift, drag, and pitching moment of the aircraft
C_L, C_D, C_M	Total lift, drag, and pitching moment coefficients of the aircraft
MTOW	Maximum take-off weight
OEW	Operating empty weight

*Ph.D. Candidate, AIAA Student Member, tom.reist@utoronto.ca

†Professor and Director, J. Armand Bombardier Foundation Chair in Aerospace Flight, Associate Fellow AIAA, dwz@oddjob.utias.utoronto.ca

I. Introduction

With concern about both the exhaustion of fossil fuels and their contribution to climate change, the need for more fuel efficient aircraft is becoming more pronounced for both economic and environmental reasons. There have been great advances in transport aircraft efficiency since the introduction of the de Havilland Comet in 1952, and the conventional tube-and-wing (CTW) configuration remains to this day. However a step change in fuel efficiency may be possible through novel configurations. One such configuration that has received much attention in recent years is the hybrid, or blended, wing-body (BWB).

The BWB has the potential to be more aerodynamically efficient than conventional configurations due to its potential for reduced wetted area, better area ruling, reduced interference drag, and intrinsically higher span.[1] Structurally, the aerodynamic lifting loads are more closely aligned with the weight of the aircraft due to the lifting fuselage, leading to reduced bending loads in the main wing structure and therefore lower structural weight.[1] However, the design of a non-cylindrical pressure vessel is challenging.[2–4] The use of a well integrated propulsion system, such as boundary-layer-ingestion or distributed propulsion, can lead to propulsive efficiencies and reductions in noise. The absence of an empennage makes stability and control potentially challenging,[5,6] and certification and customer acceptance must also be addressed.

Several large projects around the world have focused on the development of the BWB design. In the United States, Boeing and NASA have been involved in the identification and development of enabling technologies required for the BWB design,[1–3,5,7,8] with contributions leading to the X-48 flight demonstrators. A BWB design focused on noise reduction has been developed as part of Cambridge and MIT's 'Silent' Aircraft Initiative.[9,10] In Europe, two of the main projects relating to BWB design are the Multidisciplinary Optimization of a BWB[11] and the Very Efficient Large Aircraft[12] projects.

The focus of the above studies has been on large capacity aircraft. The BWB's intrinsic design features lend themselves well to large aircraft. However this design may also offer advantages across a range of aircraft sizes. Nickol examined a series of BWB aircraft ranging from 98-400 passengers.[7] As expected, the fuel burn benefit was most significant for the larger aircraft, with the 98 passenger aircraft burning more fuel than a comparable tube-and-wing aircraft. However, the fuel burn disadvantage of the small BWB was highly sensitive to drag. Thus, if a suitable drag reduction can be achieved, perhaps through a shape significantly different than that assumed by Nickol, the BWB could potentially be more fuel efficient than the tube-and-wing aircraft for a variety of aircraft classes. Such a drag reduction could potentially be obtained through high-fidelity aerodynamic shape optimization (ASO).

ASO has been applied to BWB design at a variety of fidelity levels, primarily to large aircraft. The work of Peigin and Epstein,[13] Qin et al.,[14] Le Moigne and Qin,[15] and Lyu and Martins[16,17] all focused on optimization of very large aircraft. A small BWB was optimized by Kuntawala et al.;[18] however this optimization was based on the Euler equations, so viscous drag was not captured. Previous work by the present authors includes single and multipoint optimization of a regional-class BWB using both the Euler and RANS equations.[19] The impact of trim and stability constraints on the optimal BWB design at both on- and off-design conditions was examined. It was demonstrated that, for cruise, these constraints lead to a small performance penalty at on-design conditions through tailoring of the aerodynamic shape and aircraft weight distribution, while performance degrades significantly at off-design conditions. All of the above works optimized BWBs in isolation, with no comparison to conventional designs under the same assumptions. In addition, the amount of geometric freedom given to the optimizer was, in most cases, limited. This effectively constrained the resulting designs to fall close to the classical BWB shape.

Through exploratory ASO, the present authors developed a lifting-fuselage configuration (LFC) for regional-class aircraft, which was found to be more efficient than both CTW and BWB designs in this class.[20] A low-fidelity argument for the configuration that minimizes wetted area, and how the optimal shape changes with aircraft size, was presented by the authors.[21] The present study aims to 1) characterize the relative performance of BWB and CTW aircraft across a range of aircraft sizes, and 2) to examine the potential of the LFC design for a range of aircraft sizes by comparing its performance to that of CTW and BWB designs.

A. Aerodynamic Shape Optimization Framework

The aerodynamic shape optimization framework comprises three main components: 1) a multiblock Newton-Krylov-Schur solver for the Euler[22] and RANS equations with the one-equation Spalart-Allmaras turbulence model,[23] 2) a B-spline geometry parameterization which is coupled with an integrated linear elasticity mesh movement strategy,[24] and 3) the gradient-based optimizer SNOPT,[25] with gradients calculated using the discrete adjoint method.[24,26]

The flow solver is a parallel implicit solver that uses summation-by-parts operators for spatial discretization and simultaneous approximation terms for the imposition of boundary and block interface conditions. The Krylov subspace method Generalized Minimum Residual (GMRES) is used with approximate Schur preconditioning in an inexact Newton method for the solution of the discrete equations. Details of the flow solver can be found in Hicken and Zingg[22] and Osusky and Zingg.[23]

At each optimization iteration for which a geometric shape change occurs, the computational grid must be moved to reflect this change. To accomplish this, each block of the computational grid is fitted with a B-spline volume. The design variables for the optimization can be either the B-spline control points on the aerodynamic surface, or the B-spline parameterization can be embedded within a free-form deformation volume that can be controlled through 'axial curves', as described by Gagnon and Zingg.[27] For this work direct control of the B-spline control points is used. As the B-spline control points on the aerodynamic surface are moved, each B-spline volume block is treated as a linear elastic solid, for which a finite-element solution is obtained to define the new shape of the B-spline volume. The computational grid is then recovered from this new B-spline volume. This method has been found to be very robust for large shape changes while being relatively inexpensive. Details can be found in Hicken and Zingg.[24]

Due to the high cost of evaluating the flow equations, a gradient-based optimizer is used for optimization, as gradient-based optimizers typically require fewer function evaluations than genetic algorithms.[28] The penalty paid is that for multimodal optimization problems only a local optimum may be found. This can be addressed using the gradient-based global optimization techniques proposed by Chernukhin and Zingg.[29] However, such an approach is not used here, so the optima reported represent local optima and possibly not the global optimum. The gradients of the objective and constraints are evaluated using the discrete adjoint method. This method is advantageous for problems with many more design variables than constraints, as the cost of the gradient evaluation is nearly independent of the number of design variables. The number of adjoint solutions required is proportional to the number of objectives and constraints that depend on the flow properties. Since this can require significant computational cost for practical problems, an efficient method of solving the linear system of the adjoint problem is required. For this, a modified, flexible version of the Generalized Conjugate Residual with Orthogonalization and Truncation (GCROT) algorithm is used.[30] The gradient-based optimizer SNOPT is used, as it allows for the solution of large-scale constrained problems. Details of the adjoint method and its integration with the flow solver and mesh movement are given by Hicken and Zingg,[24] while the details of SNOPT are described by Gill et al.[25]

The above algorithm has been used extensively for ASO of various problems including induced drag minimization of non-planar wings,[27,31] optimization of wings in transonic[27,32] and turbulent flows,[26] the design of low-sweep wings,[33] investigation of the multimodality of ASO problems,[29] and the optimization of unconventional[34–37] and BWB[18–21] aircraft. This framework has also been extended to aerostructural optimization.[38,39]

II. Design Problem

Four classes of aircraft are considered, with the aircraft used to define the associated reference mission in parentheses:

1. 100-passenger regional jet transport (Embraer E190[40])
2. 160-passenger narrow-body transport (Boeing 737-800[41])
3. 220-passenger mid-size transport (Boeing 767-200ER[42])
4. 300-passenger wide-body transport (Boeing 777-200LR[43])

For each class, CTW and BWB designs are created using a low-fidelity conceptual design tool that incorporates aerodynamic and weight-and-balance analyses using the methods of Torenbeek,[44] Kroo,[45] and Raymer.[46] For the BWB designs, the weight of the center-body structure is obtained using the method of Bradley.[47] The methods used to obtain the remaining structure, systems, fuel, and operational item weights for the BWB are the same as those used for the CTW aircraft. The same low-fidelity aerodynamic models are used for both aircraft, with the BWB being treated as a wing. This weight estimation methodology has been evaluated for a series of CTW designs against publicly available data, and for BWB aircraft against the results of Nickol.[7] For this work, all estimates are based on technology levels similar to those of the reference aircraft, e.g. existing engines, primarily aluminum construction, no active flow control, etc.

Since most aircraft are not typically operated at their maximum range and/or payload condition for most missions, this study will examine their use for a nominal mission. The nominal mission for the regional jet is chosen to be a 500 nmi route with a full passenger payload of 100 PAX. The narrow-body nominal mission is a 1,000 nmi route with a full passenger payload of 160 PAX. The mid-size transport nominal mission is a 3,000 nmi mission with full passenger payload, 220 PAX, with an additional 12,800 lb of revenue cargo, corresponding to 50% utilization. Finally, for the wide-body, a 6,000 nmi nominal mission with full, 300 PAX, passenger payload and 50% revenue cargo of 37,500 lb is used. The nominal cruise speeds are Mach 0.78, 0.79, 0.80, and 0.84, respectively, which are chosen to be representative of the reference aircraft. All designs are chosen to have an initial cruise altitude of 36,000 ft for the nominal mission, which is within a typical range for the reference aircraft. The same altitude is used for all classes, and for both the CTW and BWB designs, to allow for comparison at the same conditions. The optimal cruise altitude is dependent on wing loading, engine performance, buffet, etc., and can thus vary between classes. The effect of cruise altitude is examined in Section V.

All of the designs presented in this section are used as the starting point for the high-fidelity ASO presented in the following sections, upon which all performance comparisons will be made. Both the CTWs and BWBs will be optimized in the same manner, subject to the same variables, constraints, and assumptions, which will allow a direct performance comparison between the performance of the two concepts. CTWs are created, and later optimized, for the regional, narrow-body, and wide-body classes. No CTW is explored for the mid-size case. The choice to exclude the mid-size CTW is based on the fact that the other classes provide more relevant information. The regional and narrow-body-class BWBs have not been thoroughly studied in the literature, and thus having performance comparisons for these cases is important. The wide-body represents the other end of the size spectrum, and it is included to investigate the scaling of both the CTW and BWB performance with aircraft size. The mid-size BWB is included to help establish the trend of optimal BWB shape with size, as will be discussed in Section IV.

For each class of aircraft, a BWB is created to reflect shapes typically seen in the literature. The determination of an appropriate span is, however, not obvious. Due to the span loading provided by the lifting center-body, larger spans are possible for the BWBs than the CTWs. Wing weight scales strongly with span, and while there are of course other considerations, such as sweep, wing area, high-lift devices, thickness, etc., which affect the wing weight, span is a dominant factor. Thus, we introduce the concept of the 'bending span'. This is taken as the portion of the span which is primarily subjected to bending loads. For the CTW aircraft, this is taken as $b_{\text{bend}} = b - D_{\text{fuse}}$, where b is the total span, and D_{fuse} is the fuselage diameter. For BWB aircraft, the bending span is taken as the span of the wing in isolation and is defined as $b_{\text{bend}} = b - w_{\text{cb}}$, where w_{cb} is the width of the center-body. The bending span will be used to determine an appropriate span by serving as a low-order surrogate for wing weight. The assumption is then made that a BWB could feasibly be created which has a bending span equivalent to that of a similarly sized CTW. This is a conservative assumption for BWB wings since it does not account for the load relief provided by the increased lift carried by the center-body. This bending span is used to create BWBs by choosing the spans such that the bending spans are close to those of the equivalent CTWs. If this results in a span coming close to a gate limit, the gate limit value is used since this is a more well defined rationale for the span than the bending span argument.

For the regional-class BWB, a 130 ft span design, referred to as the BWB100, is created which has a bending span similar to that of the CTW100. For the narrow-body, mid-size and wide-body-class BWBs, spans are chosen which are at the gate limit of the next gate class; the BWB160, BWB220, and BWB300 designs are created with 170 ft, 213 ft, and 262 ft spans, respectively. For these three classes, the equivalent bending span argument yields spans that are close to gate limits, and the spans shown above are thus chosen so that each design resides at a gate limit. This results in bending spans that are within 5% of those of the equivalent CTWs. For each class, the BWB design requires a gate one size larger than its CTW counterpart.

Each aircraft is sized for its design mission, i.e. the maximum range and payload combinations on the envelope of the payload-range diagram for the reference aircraft. These models are then used to estimate the aircraft weights and center of gravity location at the beginning of the nominal mission cruise, which serves as the operating point for the high-fidelity optimization. The conceptual design models are shown in Figure 1 with basic design information given in Tables 1 and 2.

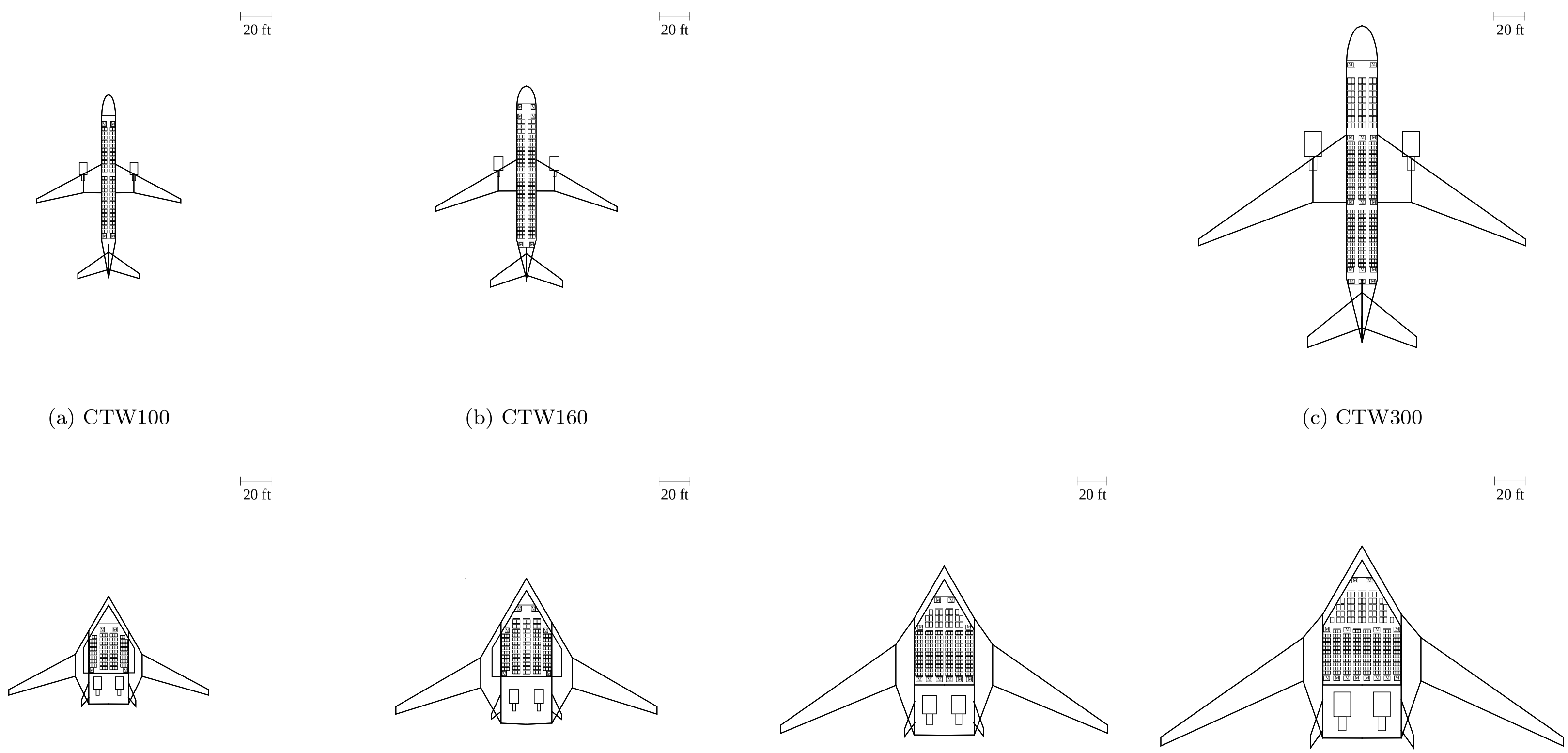

(a) CTW100 (b) CTW160 (c) CTW300

(d) BWB100 (e) BWB160 (f) BWB220 (g) BWB300

Figure 1: Planforms for each of the baseline designs.

Table 1: Baseline CTW design information.

Design	PAX	Gate	Span [ft]	Bending span [ft]	Reference area [ft^2]	Aspect ratio [–]	MAC [ft]	OEW [lb]	MTOW [lb]	Weight* [lb]
CTW100	100	C	94	85	1,000	8.9	13.1	59,200	105,800	91,500
CTW160	160	C	118	105	1,350	10.3	14.3	88,100	173,900	143,300
CTW300	300	E	213	193	4,990	9.1	30.3	330,900	775,500	633,900

* At the start of nominal mission cruise

Table 2: Baseline BWB design information.

Design	PAX	Gate	Span [ft]	Bending span [ft]	Reference area [ft^2]	Aspect Ratio [–]	MAC [ft]	OEW [lb]	MTOW [lb]	Weight* [lb]
BWB100	100	D	130	88	2,840	9.7	41.1	73,500	121,200	106,600
BWB160	160	D	170	110	5,140	9.0	55.9	126,300	217,300	185,300
BWB220	220	E	213	150	7,260	9.4	62.5	221,200	432,600	355,400
BWB300	300	F	262	185	9,780	11.0	70.7	417,000	826,800	700,500

* At the start of nominal mission cruise

The BWB's interior cabin height for each class is 79 inches. This is the same as the interior height of the regional jet CTW, but smaller than that of the narrow-body, mid-size, and wide-body CTWs. While the cabin height of a CTW is intrinsically linked to the cabin width due to the cylindrical fuselage, this is not the case for BWBs so the cabin height can be chosen independently of width. For this work, all of the BWB cabin heights are selected to adequately accommodate an adult standing in the aisles.

The regional-class BWB has the cargo located outboard of the passenger cabin, while the other three classes have under-floor cargo. It was found that under-floor cargo for the regional-class BWB requires a prohibitive chord increase to attain an appropriate thickness-to-chord ratio, and is thus not optimal. For the narrow-body and above, cargo outboard of the passenger compartment results in an unnecessary increase in wetted area, as under-floor cargo can be accommodated without a prohibitive thickness-to-chord ratio.

The assumption is made that the BWB designs will require some form of lateral stabilizer. It is assumed that two vertical stabilizers outboard of the engines will be used so as to also provide noise shielding. These stabilizers are sized such that they have sufficient area to counteract a one-engine-inoperative yawing moment, given the same vertical stabilizer lift coefficient as the baseline conventional aircraft.

The same engines are used for the BWBs as for the CTWs, which are those of the reference aircraft, where simple pylon mounting is assumed such that the BWBs receive no credit for advanced engine installation, such as boundary layer ingestion.

III. Aerodynamic Shape Optimization Studies

Based on the designs presented above, full three-dimensional surface models are created using the geometry toolbox developed by Gagnon and Zingg.[34] The baseline CTW wings are untwisted and use the SC(2)-0012 section at the root and crank, and the SC(2)-0010 section at the tip. The baseline BWB bodies use SC(2)-0014 sections, with SC(2)-0012 and SC(2)-0010 sections at the wing root and tip, respectively. Since the initial center-body airfoils are not designed specifically for BWB use, in order to maintain sufficient thickness up to 70% chord to house the cabin, a 14% thick section is used on the center-body. This is an inefficient packing of the cabin within this section, so the optimizer will be used to design a more appropriate section that has a lower maximum thickness-to-chord ratio, which is maintained over a larger fraction of the chord.

The vertical stabilizers, nacelles, and pylons are not included in the three-dimensional models. The vertical stabilizers are not included as they are sized by conditions other than cruise, which are not included in the high-fidelity optimization. Their drag contribution is accounted for post-optimization by one of two methods: 1) for the regional-class aircraft, three-dimensional models of the vertical stabilizers are created and analyzed with the high-fidelity solver in isolation; 2) to reduce cost for the remaining classes, the Mach

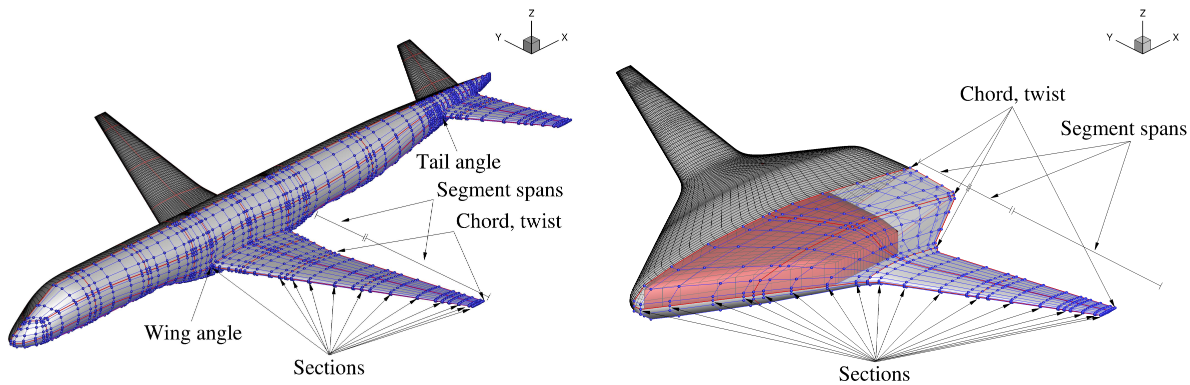

(a) CTW design variables

(b) BWB design variables

Figure 2: Surface geometries for the regional-class CTW and BWB baselines showing both the surface CFD mesh and control mesh along with the types and locations of the geometric design variables. The upper surface of the BWB body is transparent to reveal the polyhedron that encloses the cabin. (Not shown to the same scale.)

number corrected version of the Prandtl-Schlichting[46] skin friction equation is used to estimate the skin friction drag of the vertical stabilizers, and form drag is accounted for with a form factor of 1.22 obtained from the RANS solution of the regional-class vertical stabilizers. Interference drag between the vertical stabilizers and fuselage/center-body is neglected.

The BWBs are optimized using grids with 1.5×10^6 nodes, and the CTWs use grids with 6.3×10^6 nodes. These grids are chosen as described in Reist and Zingg[20] so as to accurately predict the correct friction/pressure drag ratio and thus capture the drag trade-offs associated with changes in wing area. Both the BWB and CTW grids have similar near-body resolution; the CTW grids are larger as a consequence of the use of multiblock structured grids. While these grids are too coarse to provide accurate force and moment estimates, it has been found that they are capable of capturing the dominant flow features and providing a reasonable estimate of the friction/pressure drag ratio, and thus properly designing the shape.[29,48] To determine the final force and moment coefficients of the optimized designs, grid convergence studies are performed for each optimized design. For each design, a sequence of two additional grids with 2 and 4 times as many nodes as the optimization grid is created, and Richardson extrapolation is used with an assumed order of accuracy of two to determine the grid-converged performance estimates. For the regional-class designs an additional grid level is added to the sequence to improve accuracy to allow for comparisons between designs with very similar performance. Unless otherwise stated, all the performance results presented in the remainder of this work are Richardson extrapolated estimates for grid-converged performance, and include the drag contribution from the vertical stabilizers.

A. Optimization Problem Definition

RANS-based aerodynamic shape optimization is performed at conditions that correspond to the start of the cruise segment of the nominal missions. The starting geometries, which have untwisted wings and use symmetric sections, are initially infeasible and have poor performance. The objective of the optimization is to minimize drag subject to lift and pitching moment constraints, in addition to geometric constraints described below. This work investigates aerodynamically optimal configurations that offer minimum drag for each class of aircraft. Naturally, aircraft design is also driven by additional considerations which would need to be taken into account during design. The impact of design changes made by the optimizer on structural weight, aeroelastic behaviour, flight dynamics, etc. are not modelled. Rather, since aerodynamic performance is tightly coupled to other disciplines, the optimization problem design variables and constraints are constructed so as to limit geometric changes which have a significant impact on other disciplines, while allowing enough freedom to achieve aerodynamically optimal designs. The following description applies to the optimization for each class.

The surface CFD grid and the geometry parameterization are shown in Figure 2. The background surface shows the CFD grid, while the foreground surface shows the B-spline control grid, and the locations of the

Table 3: Design variables and constraints. Bounds given as percentages are deviations from the initial values. Numbers in parentheses are the number of each type of variable/constraint.

	CTW			BWB		
Variables	$-3° \leq$	AoA (1)	$\leq +3°$	$-3° \leq$	AoA (1)	$\leq +3°$
	$-5° \leq$	Wing angle (1)	$\leq +5°$			
	$-5° \leq$	Tail angle (1)	$\leq +5°$			
	$-75\% \leq$	Segment span (2)	$\leq +75\%$	$-75\% \leq$	Segment span (3)	$\leq +75\%$
				$0° \leq$	Transition region sweep (1)	$\leq 85°$
	$-50\% \leq$	Chord (2)	$\leq +50\%$	$-50\% \leq$	Chord (4)	$\leq +50\%$
	$-10° \leq$	Twist (2)	$\leq +10°$	$-10° \leq$	Twist (3)	$\leq +10°$
	$-200\% \leq$	Section shape[1](264)	$\leq +200\%$	$-200\% \leq$	Section shape[1](396)	$\leq +200\%$
		Total effective design variables: 273			Total effective design variables: 408	
Constraints	$-20\% \leq$	t/c (132)	$\leq +50\%$	$-20\% \leq$	t/c (198)	$\leq +50\%$
	$1.25V_{\text{fuel}} \leq$	V_{wing} (1)		$1.25V_{\text{fuel}} \leq$	V_{wing} (1)	
	$-0\% \leq$	Span (1)	$\leq +0\%$	$-0\% \leq$	Span (1)	$\leq +0\%$
	$-0\% \leq$	Wing sweep (2)	$\leq +0\%$	$-0\% \leq$	Wing sweep (1)	$\leq +0\%$
					Cabin shape (2050)	
		$L = W$ (1)			$L = W$ (1)	
		$C_M = 0$ (1)			$C_M = 0$ (1)	

[1] The amount by which the control points defining the sections can move normal to the chordline, as a percentage of their initial distance from the chordline.

different geometric design variables are indicated. A portion of the BWB's upper surface is transparent to show the cabin shape. The method by which the B-spline control points are manipulated by the design variables is described in Osusky et al.[26] The specific design variables and constraints are summarized in Table 3 and described below.

The angle-of-attack is a design variable for both configurations and is limited to $\pm 3°$ due to deck angle requirements. The incidence angle of the CTW wing and tail are free to vary between $\pm 5°$. The CTW wing is divided into two segments, one inboard and one outboard of the crank. The BWB consists of three segments, one over the cabin, one transition segment between the edge of the cabin and the wing root, and one for the wing. The span of each of these segments can vary, but the total span remains fixed. The quarter-chord sweep angles of the CTW wing and the BWB wing are fixed. The sweep angle of the transition region of the BWB, between the cabin and the wing, is free to vary such that the optimizer can position the wing to minimize trim drag. For the CTW, the wing chord and twist are allowed to vary at the crank and tip, with linear variation between. For the BWB, the chord is variable at the centerline, and the chord and twist are variable at the outboard edge of the cabin, wing root, and tip, with linear variation between. The CTW and BWB have section control at 12 and 18 span-stations respectively, at each of which there are 22 section variables, 11 for each of the lower and upper surfaces. For each pair of lower and upper surface section shape variables there is a corresponding thickness constraint to prevent the thickness decreasing by more than 20% of the initial value. For the CTW, geometric changes to the fuselage caused by changes of the wing/tail root are handled via the method described in Osusky et al.[26] The volume of both the CTW and BWB wings is constrained such that sufficient volume exists in the wings for fuel, with the required volume being taken from the low-fidelity sizing result, which gives 30,000 lb, 46,500 lb, 161,000 lb, and 305,000 lb of fuel for each class, respectively. It is assumed that 80% of the outer mold line volume is usable for fuel tanks. The outer mold line of the BWB is constrained such that it does not violate the specified BWB cabin shape, shown in Figure 2(b).

Lift is constrained to be equal to the weight at the start of cruise, and the pitching moment about the center of gravity must be zero. There are a total of 273 effective design variables for the CTW, and 408 for the BWB. The lift target is not updated during the optimization in response to geometric changes. While changes to weight during the optimization could be captured using the relations used for initial sizing, which are primarily functions of geometry, this is not done due to uncertainties in the accuracy of these equations. These inaccuracies could be exploited by the optimizer to lighten the aircraft in a way which is unrealistic. The aim is to avoid contaminating the high-fidelity optimization with low-fidelity approximations which can be exploited by the optimizer. As a check, after each optimization, new low-fidelity models are built to reflect any geometric changes, and the resulting changes in OEW are typically less than 2%.

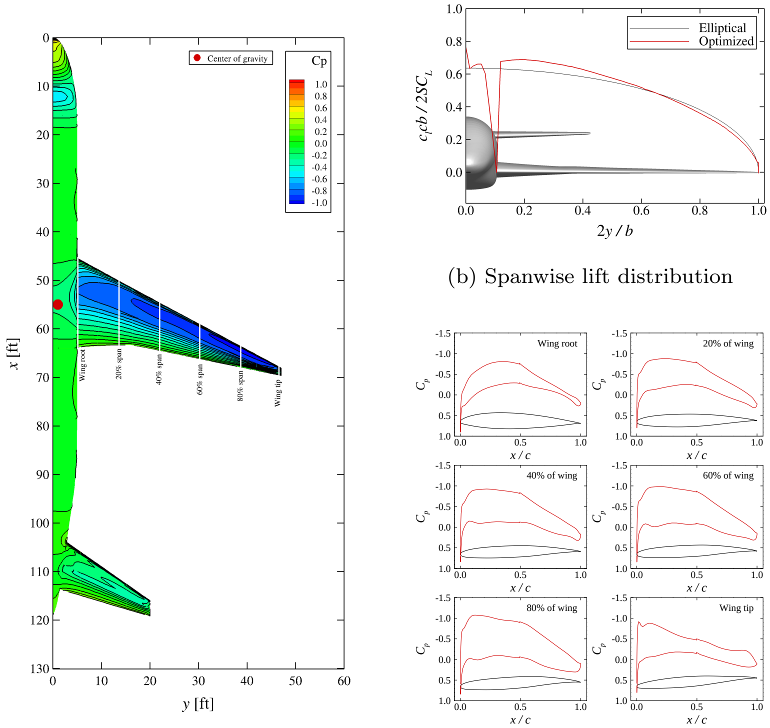

(a) Surface pressure distribution

(b) Spanwise lift distribution

(c) Sectional pressure distributions

Figure 3: Solution information for the optimized CTW100-1 design.

Table 4: Optimized CTW performance at the start of cruise.

Design	Weight [lb]	S [ft^2]	C_L [–]	C_D [–]	L/D [–]	D/q_∞ [ft^2]	Drag [lb]
CTW100-1	91,500	935	0.481	0.0243	19.8	22.7	4,621
CTW160-1	143,300	1,370	0.501	0.0247	20.3	33.8	7,059
CTW300-1	633,900	5,209	0.515	0.0220	23.4	114.7	27,090

B. CTW optimization

The results of the CTW optimizations are shown in Figures 3-5. The optimized designs are referred to by the suffix '-1'. As can be seen from the sectional pressure profiles[a], all designs are shock free. While each design started with symmetric sections, the sectional cuts show that the optimizer has found supercritical designs, which are most pronounced for the CTW300-1, which has the highest Mach number. The spanwise lift distributions are nearly elliptical on the outboard portion of the wing, but deviate from the ideal distribution inboard, likely due to the presence of the fuselage. For each class, the maximum section thickness goes to its lower bound along most of the span, with the exception of the wing root. Except for the CTW300-1, which increases the wing area by increasing the tip chord, the wing volumes also go to their lower bound. The CTW300-1 adds the maximum 10° of washout at the tip. These are the only geometric constraints that are active at the solution. The angle-of-attack for each class goes to its upper bound of 3.0°.

The performance of each design is shown in Table 4. The lift-to-drag ratios increase with aircraft size as expected due to the increasing wetted aspect ratios. The lift-to-drag ratios are close to what would be expected for modern CTW aircraft, but slightly higher, since nacelle and excrescence drag are not considered, and these designs are point-optimized for this condition. These numbers will form the basis for performance comparisons with the BWBs.

[a]The small pressure discontinuities seen at the mid-chords are due to the presence of a block boundary and the use of simultaneous approximation terms for the interface boundary conditions.

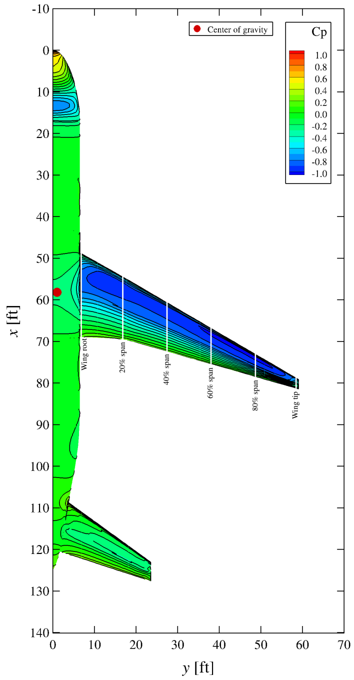

(a) Surface pressure distribution

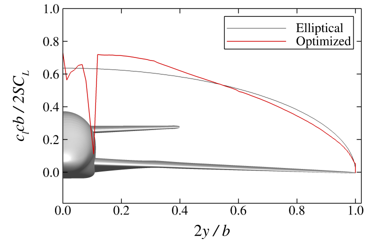

(b) Spanwise lift distribution

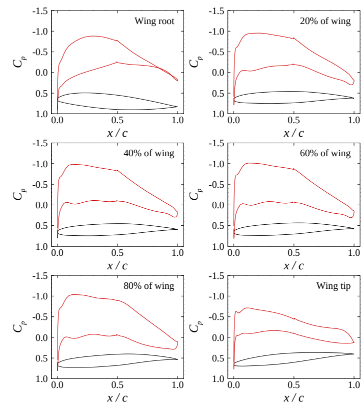

(c) Sectional pressure distributions

Figure 4: Solution information for the optimized CTW160-1 design.

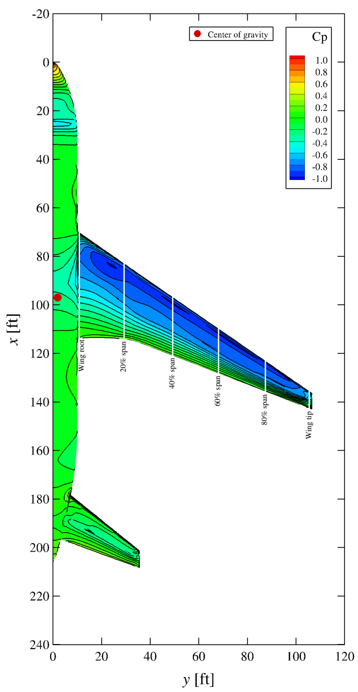

(a) Surface pressure distribution

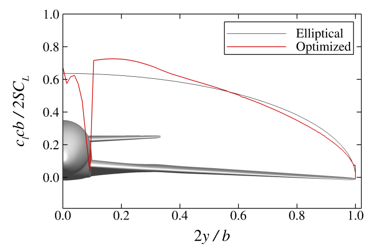

(b) Spanwise lift distribution

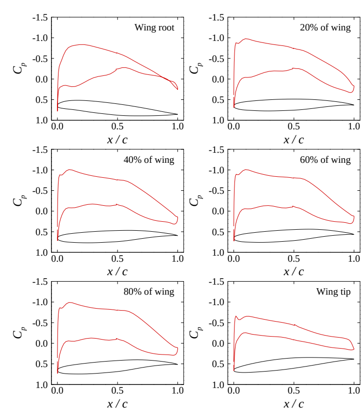

(c) Sectional pressure distributions

Figure 5: Solution information for the optimized CTW300-1 design.

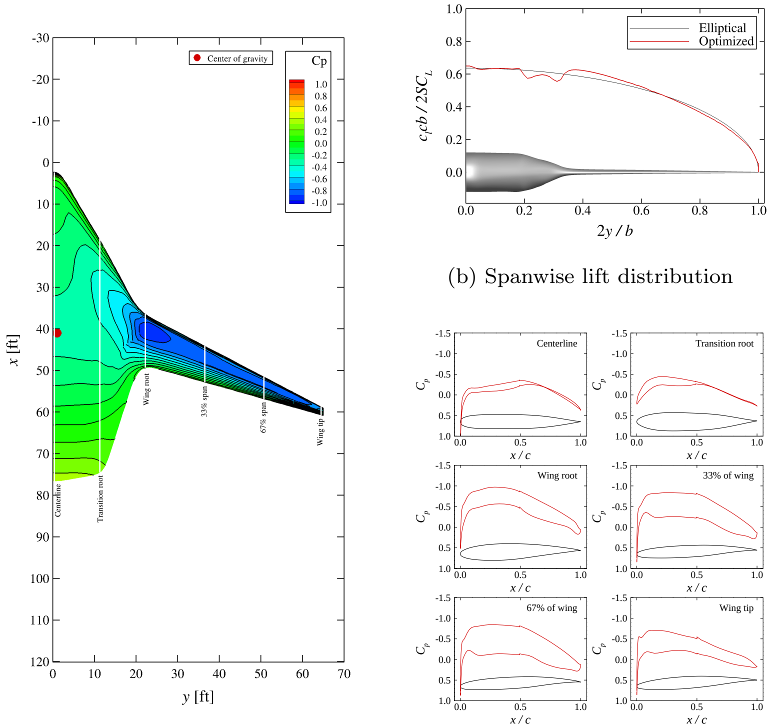

(a) Surface pressure distribution

(b) Spanwise lift distribution

(c) Sectional pressure distributions

Figure 6: Solution information for the optimized BWB100-1 design.

C. BWB optimization

For each optimized BWB, identified by the suffix '-1', the optimized geometry, surface pressure distribution, spanwise lift distribution, and sectional pressure distributions are shown in Figures 6-9. For each class, the action of the optimizer is to closely wrap the outer mold line of the body around the prescribed cabin shape to minimize wetted area while, in some cases, increasing the chord on the center-body to decrease the maximum thickness-to-chord ratio. For each class, the wing volume and maximum thickness on the wing go to their lower bounds. With the exception of the wide-body-class BWBs, the tip chords go to their lower bounds. In addition to the cabin shape constraint, these are the only geometric constraints that are active at the solution. The BWBs all have a final cruise angle-of-attack of between 2.5° and 3.0°.

It is known from linear aerodynamics that an elliptical spanwise lift distribution produces minimum induced drag for a planar wing. When nonlinear considerations are present the same statement cannot be made with such certainty. However, as demonstrated by Osusky et al.,[26] a lift distribution close to elliptical can be expected for practical wings in transonic, viscous flows. The spanwise lift distributions shown in Figures 6(b)-9(b) show near-elliptical behaviour on the wings. There is some deviation, which increases with aircraft size, as a likely consequence of the higher Mach number. As pointed out by Qin et al.[14,49] this can be expected for transonic problems, particularly those with high local lift coefficients, as the optimizer must balance the reduction in induced drag with wave drag. Additional considerations such as the fact that the wings are swept and that they contribute to the trim of the aircraft also place further restrictions on the lift distribution that is optimal for total drag. For each design, there is significant deviation from an elliptical distribution at the wing-body junction due to the rapid change in thickness and chord; this is particularly pronounced for the BWB160-1 where the optimizer has decreased the span of the transition region such that the thickness and chord changes occur particularly rapidly.

Figures 6(c)-9(c) show the sectional pressure distributions at the centerline, the transition root (which is at the outboard edge of the cabin where the chord begins to decrease rapidly), and four stations between the wing root and tip. The designs are shock and nearly separation free. The sectional pressure distributions show the manner in which the optimizer trims the BWBs. The center-body sections are fore-loaded such that they carry almost all of their lift ahead of the center of gravity, with little to no inefficient reflex required,

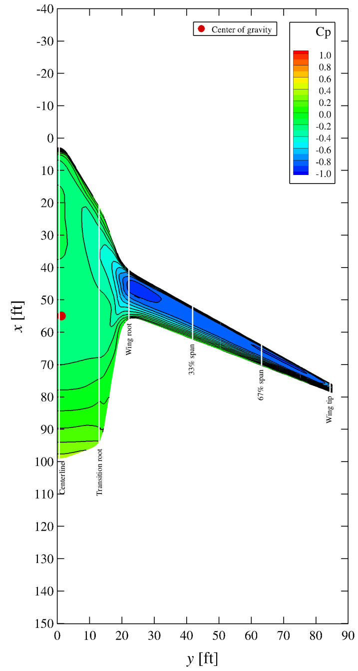

(a) Surface pressure distribution

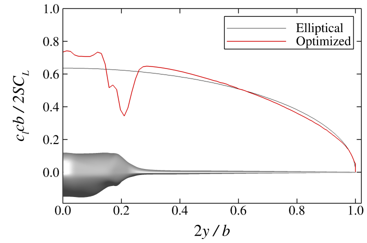

(b) Spanwise lift distribution

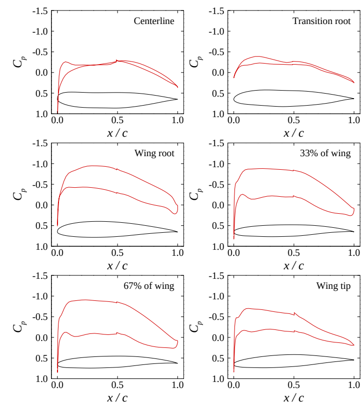

(c) Sectional pressure distributions

Figure 7: Solution information for the optimized BWB160-1 design.

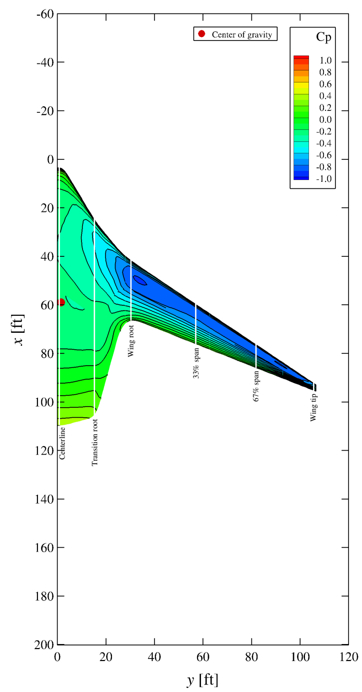

(a) Surface pressure distribution

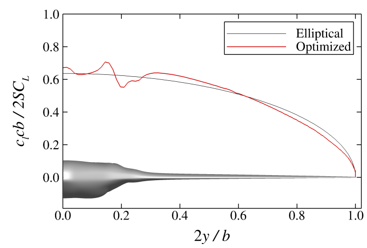

(b) Spanwise lift distribution

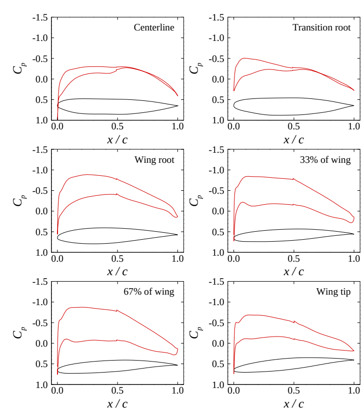

(c) Sectional pressure distributions

Figure 8: Solution information for the optimized BWB220-1 design.

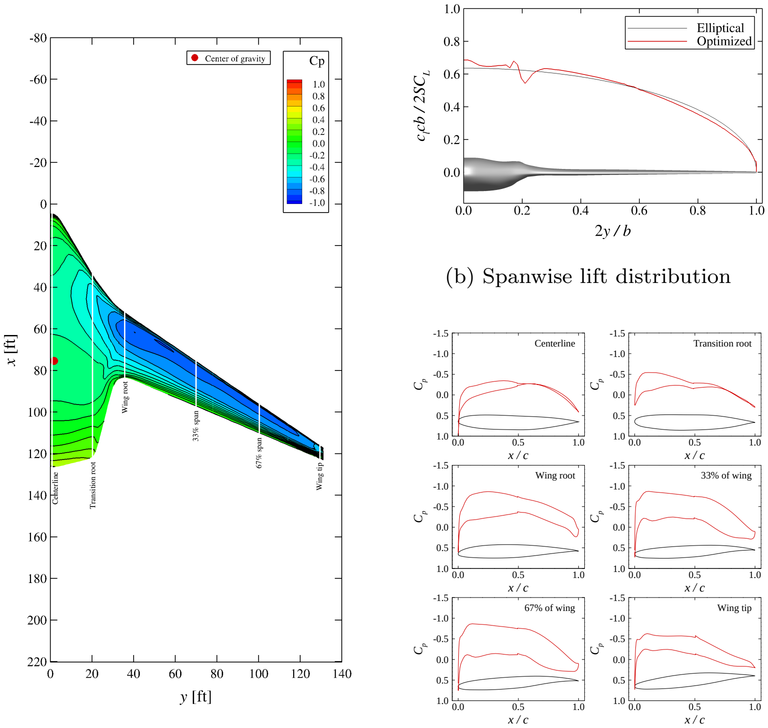

(b) Spanwise lift distribution

(a) Surface pressure distribution

(c) Sectional pressure distributions

Figure 9: Solution information for the optimized BWB300-1 design.

Table 5: Optimized BWB performance at the start of cruise. Fuel-burn is that of the cruise segment, and is given relative to the optimized CTW in each class.

Design	Weight [lb]	S [ft^2]	C_L [–]	C_D [–]	L/D [–]	D/q_∞ [ft^2]	Drag [lb]	Relative fuel-burn [%]
BWB100-1	106,600	2,813	0.186	0.0081	23.0	22.8	4,635	+0.6
BWB160-1	185,300	3,989	0.222	0.0083	26.6	33.3	6,966	−1.4
BWB220-1	355,400	6,388	0.260	0.0090	28.9	57.5	12,298	–
BWB300-1	700,500	9,467	0.313	0.0104	30.0	98.8	23,350	−10.9

with the exception of the BWB160-1. The optimizer has found the same trim mechanism as described by Sargeant et al.[50] The optimizer trims the designs primarily through the center-body design since the large chord implies that small changes in the local sectional pitching moment coefficient produce a significant total change in the pitching moment without inducing large performance penalties associated with strongly fore-loaded sections, as noted by Mialon et al.[51] On the wing, the optimizer designs supercritical sections. While trimmed, all of the designs are longitudinally unstable, with static margins between 0% and −9.4% and would require some form of an active stability system. The impact of requiring a non-negative static margin is investigated for the regional-class BWB by Reist and Zingg.[20]

The performance of the optimized designs is given in Table 5, with two primary points to note. First, the lift coefficient, and hence wing loading, increases with aircraft size. This would suggest a higher cruise altitude is required to attain maximum lift-to-drag ratio for the smaller sizes. This will be addressed in Section V. Secondly, the lift-to-drag ratio increases with aircraft size. This is partially a consequence of the larger designs operating closer to their optimal lift coefficient, and partly a result of the higher wetted aspect ratio as discussed in the next section.

Comparing the performance given in Tables 4 and 5, it can be seen that the drag and fuel-burn of the smaller BWBs are close to that of the CTWs, while the optimized wide-body-class BWB burns almost 11% less fuel during cruise than the CTW300-1. Cruise fuel-burn is calculated via the Breguet range equation, rearranged as

$$W_{\text{fuel}} = W_0 \left[\exp\left(\frac{R c_T}{V L/D} \right) - 1 \right] \tag{1}$$

where W_0 is the non-cruise fuel portion of aircraft weight at the start of cruise, i.e. the weight at the end of cruise, R is the cruise range, c_T is the thrust-specific fuel-consumption, L/D the lift-to-drag ratio, and V the cruise speed. While the magnitudes of the relative performance differ from those of Nickol[7] due to different assumptions with respect to technology levels, the trend is the same, in that a fuel-burn benefit is seen only for the larger BWB sizes.

One of the oft-quoted benefits of the BWB concept is its lower wetted area compared to equivalent CTW designs, particularly for large aircraft. However, the regional and narrow-body-class BWBs, the BWB100-1 and BWB160-1, have 14-18% *higher* wetted area than the CTW100-1 and CTW160-1, respectively. The wetted area for the wide-body BWB300-1 is 8% lower than that of the CTW300-1. This motivates the question, which forms the basis for the next section: Is there a different BWB configuration that is more beneficial for smaller aircraft sizes?

IV. Exploratory Aerodynamic Design Through High-Fidelity Optimization

While the optimizations previously presented possessed significant geometric freedom, the specification of the cabin layout and the resulting cabin shape constraint prevented significant geometric changes from being made to the center-body, a large source of wetted area, and hence drag. Thus, to investigate alternative BWB shapes that may offer improved aerodynamic efficiency, an exploratory optimization is performed with the cabin shape constraint removed, resulting in increased geometric freedom. This study aims to find the maximum aerodynamic efficiency of the BWB concept. Thus, instead of performing lift-constrained drag minimization as with the previous cases, the optimization objective is to maximize the lift-to-drag ratio. No lift target is required, and the pitching moment constraint is not considered. This also reduces the computational cost, as only one adjoint solve is required as compared to the three in the trim-constrained cases. This exploratory optimization is performed for each class of BWB considered so as to understand how the aerodynamically optimal shape changes with aircraft size.

The starting geometry for each BWB is the baseline shape from Section II. The cabin shape constraint is replaced with requirements on the center-body area and volume. The required cabin floor area and usable cabin volume for each class of BWB are those for the baseline BWBs, which are in line with the CTW values. The assumption is made that only 50% of the projected area and volume of the center-body is usable for housing the cabin due to minimum dimension requirements; the area and volume of the center-body are constrained accordingly.

The design variables and constraints for these problems are similar to those used for the BWB optimizations presented in Section III, with some notable exceptions. The first, already mentioned, is the substitution of the cabin area and volume constraints for the explicit shape constraint. Secondly, the center-body is defined by two segments instead of the three shown in Figure 2(b), i.e. the first two segments are combined to represent the center-body.[b] Finally, the leading and trailing edges of the center-body are not required to be straight. There are a total of 425 effective design variables.

The aim of these studies is to find trends in the optimal shape rather than details. Few constraints are imposed, and these studies are intended to guide the design of BWBs which can then take additional requirements into consideration. For example, the resulting shape may have sufficient space in the center-body for the payload, but due to minimum dimension requirements cannot accommodate a practical cabin configuration; thus necessitating a manually designed center-body whose shape is guided by the exploratory result, and subsequently reoptimized.

The resulting shapes of the exploratory optimization are shown in Figure 10, and are identified with the suffix '-E1'. For all cases, the primary action of the optimizer is to minimize the wetted area. All of the area and volume constraints thus go to their lower bounds. For each case, the optimizer decreases the span of the center-body to create a more elongated shape, while the thickness is limited by transonic effects. The degree to which this occurs decreases with increasing size. The regional and narrow-body-class designs produce

[b] With the original three-segment definition, there is no justification for constraining the volume of the transition segment, and the optimizer would thus decrease the transition-span to its lower bound, leading to mesh-movement complications for some classes. For those classes which were successful, the optimal shape was similar to that with the two-segment formulation.

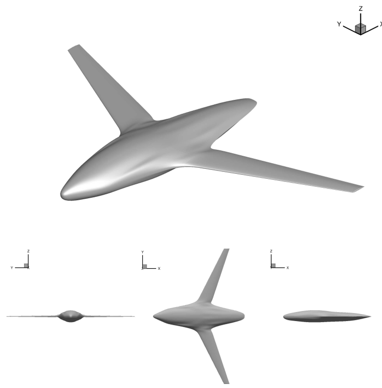

(a) BWB100-E1

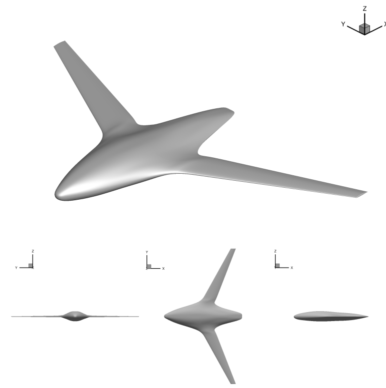

(b) BWB160-E1

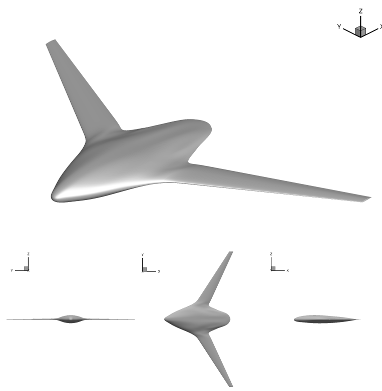

(c) BWB220-E1

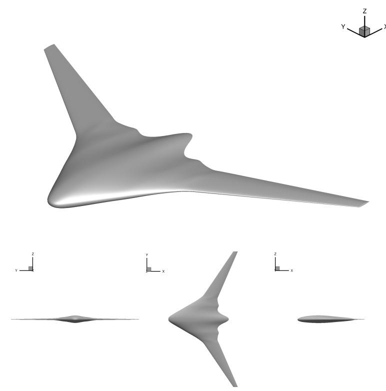

(d) BWB300-E1

Figure 10: Resulting shapes from the 'E1' exploratory optimizations. (Not shown to the same scale.)

Table 6: Summary of exploratory performance for the E1 formulation.

Design	Span [ft]	Bending span [ft]	$\mathcal{R}_{\text{wet}}$ [–]	L/D [–]
BWB100-E1	130	102	3.0	30.5
BWB160-E1	170	129	3.5	33.5
BWB220-E1	213	162	3.8	34.7
BWB300-E1	262	176	3.5	32.5

a slender center-body with distinct wings, while, for the wide-body, the center-body and wings are more blended together. The net effect is to increase the wetted aspect ratio, and hence the aerodynamic efficiency, both of which are given in Table 6. Since the goal of the exploratory optimization is the determination of an optimal shape, the exact aerodynamic performance is less important. As such, for the aerodynamic performance presented in this section, grid refinement studies are not performed. Rather, for each BWB class, the drag error between the optimization level grid and the Richardson extrapolated value is calculated from the lift-constrained drag minimization results of Section III and applied to the drag computed on the optimization level grids for the cases in this section. This gives a grid-converged performance estimate for each exploratory result, without the cost of grid refinement studies.

It can be seen in Table 6 that the wetted aspect ratio, and hence lift-to-drag ratio, increase with aircraft size. The exception to this is the wide-body, for which the choice of the 262 ft span is such that the wetted area has scaled faster than the span for this class relative to the other three. For this class of BWB, the code 'F' gate limit places a hard limit on the aerodynamic performance, as evidenced by the fact that the bending span for this class is the only one that is lower than its equivalent CTW design. Thus, even in this

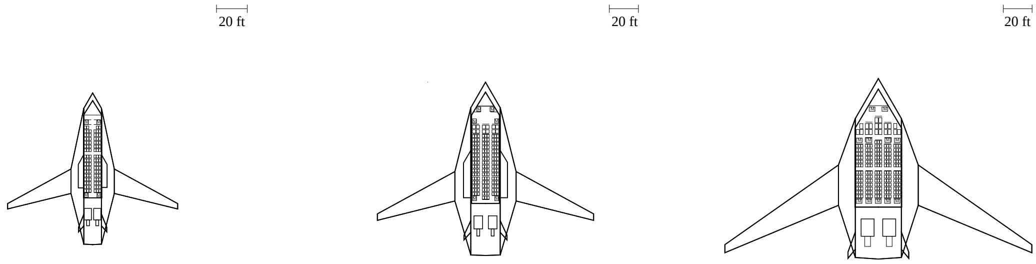

(a) LFC100 (b) LFC160 (c) LFC220

Figure 11: Planforms for each of the LFC designs.

best-case scenario, the large class of BWB would require a span greater than the maximum allowable code 'F' gate to attain a monotonic increase in aerodynamic performance with aircraft size.

All of the above designs have a fixed span. Thus, when the center-body span decreases in order to reduce the wetted area, the bending span must increase. This is beneficial from a purely aerodynamic point of view, but does not consider potential changes in structural weight. To address this, a second problem formulation is investigated, referred to with the suffix '-E2', to ensure that the E1 shapes are not purely a consequence of the problem formulation. The design variable definition is the same as for the E1 cases, except that the total span is free and the span of the wing region, i.e. the bending span, is fixed at the value corresponding to the equivalent CTW aircraft. For this problem, the action of the optimizer would be to increase the span by increasing the center-body span and decrease its chord such that the cabin area constraint would not go to its lower bound, while the thickness decreases so that the volume reaches its lower bound. In other words, the BWB reduces to a pure flying wing, one in which the thickness on the center-body is now insufficient to hold the payload. To prevent this, an average thickness constraint is introduced on the center-body, defined as $\bar{t}_{\text{cab}} = V_{\text{cab}}/A_{\text{cab}}$, where A_{cab} and V_{cab} are the cabin area and volume requirements, respectively. This constraint always goes to its lower bound and thus ensures that there is sufficient floor area, volume, and that on average the thickness is sufficient to accommodate the payload.

These optimizations produce the same trends as were found in the E1 optimizations, where the center-body spans are reduced compared to the initial shapes, although the center-body span is not reduced quite as much as in the E1 formulation. This shows that this is still the optimal configuration when the bending span is considered as a surrogate for wing weight. For this formulation, the span is not constrained by gate limits and thus the BWB300-E2 is able to increase its span, and a monotonic increase in the wetted aspect ratio is obtained across all of the classes.

A. Lifting-Fuselage Configuration Design

The exploratory results of the previous section suggest the shape for optimal aerodynamic efficiency in each class. However, while the center-body volume and area are sufficient to hold the payload if it were to take on an arbitrary shape, the imposition of minimum dimension requirements and other practical considerations lead to the shapes not being capable of holding the payload exactly as they are. Thus, these shapes are used to guide the redesign of aircraft that mimic the results of the previous section, while considering practical requirements such as a feasible cabin layout and trim.

The new designs are significantly different than the classical BWBs, and are characterized by a slender fuselage with distinct wings, where the fuselage still carries a significant portion of the lift. As such, the new designs, presented below, will be termed 'Lifting-Fuselage Configurations' (LFCs). As with the original designs, low-fidelity models of the lifting-fuselage designs are created, and are shown in Figure 11, with design information given in Table 7. As in Section II, the determination of an appropriate wing span is challenging without a full multidisciplinary design process. The bending span is again used as a surrogate for wing weight. For the regional-class design, termed the LFC100, the bending span is 88 ft for a total span of 118 ft; this is similar to the bending span of the CTW100. For the narrow-body LFC, the LFC160, the total span

Table 7: LFC design information.

Design	PAX	Gate	Span [ft]	Bending span [ft]	Reference area [ft^2]	Aspect ratio [–]	MAC [ft]	OEW [lb]	MTOW [lb]	Weight* [lb]
LFC100	100	C	118	88	3,120	8.5	62.8	71,100	118,700	104,100
LFC160	160	D	150	108	4,950	8.6	73.8	119,700	209,600	177,700
LFC220	220	E	213	158	7,630	9.4	71.2	229,600	444,400	365,500

* At the start of nominal mission cruise

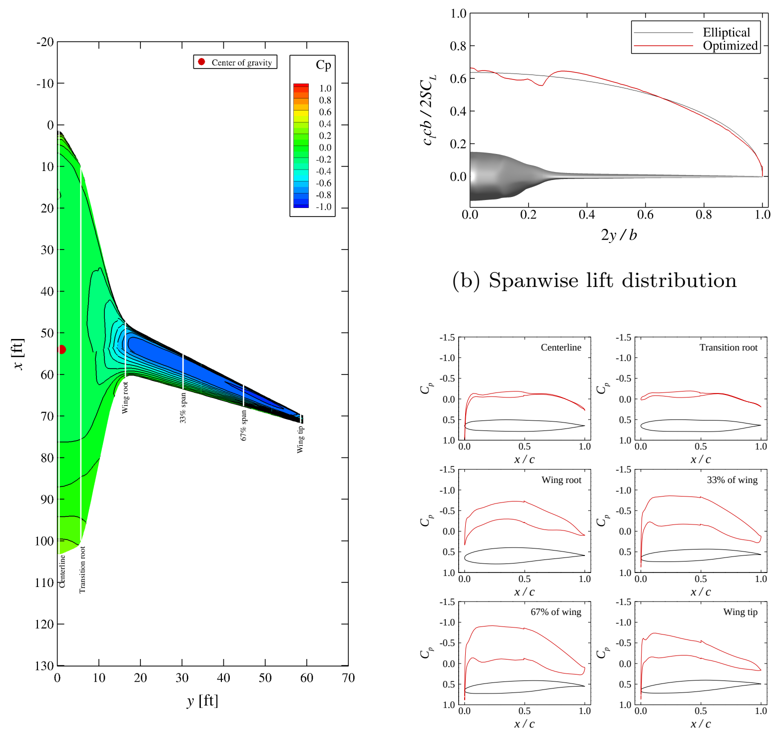

(a) Surface pressure distribution (b) Spanwise lift distribution (c) Sectional pressure distributions

Figure 12: Solution information for the optimized LFC100-1 design.

is 150 ft which gives a bending span of 108 ft, close to that of the CTW160. At a total span of 213 ft, the mid-size LFC, LFC220, has a bending span of 158 ft, similar to the CTW220. Each of these designs reside in the code 'C', 'D', and 'E' gates, respectively. An attempt was made to create a LFC for the wide-body class, but when a practical cabin layout was created, the resulting design was similar to that of the baseline classical BWB; thus, no wide-body-class LFC is pursued. The same 'home plate' center-body pressure vessel weight model is used for the LFCs as was used for the BWBs. Due to the reduced span loading of the LFC concept, an alternative structural solution, such as an elliptical or double-bubble cross section, could lead to lower center-body weight. The LFC100 and LFC160 have cargo located outboard of the passenger compartment, while the LFC220 has under-floor cargo. Use of under-floor cargo for the LFC100 and LFC160 was also investigated, however this resulted in both increased wetted area and very thick center-body sections which both lead to higher drag than the outboard cargo arrangement. Full three-dimensional CFD models are created for each of these designs in the same manner as for the BWBs. Trim-constrained drag minimization of the LFC designs is performed in the same manner as with the BWB designs. The solution information for each of the three classes is shown in Figures 12-14. The resulting performance is shown in Table 8.

As with the BWBs, each design has a lift-distribution close to elliptical, particularly on the wings. All designs are shock and nearly separation free, with most of the center-body lift being carried ahead of the center of gravity. The LFC220-1 is the only design that exhibits any reflex on the fuselage, while the LFC100-1 and LFC160-1 carry essentially no lift aft of 50% chord on the fuselage. Due to the long fuselage chord

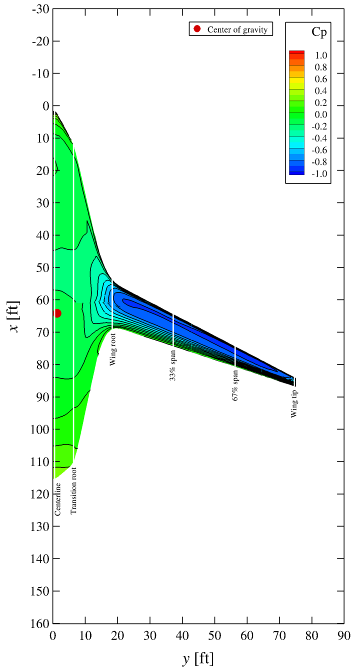

(a) Surface pressure distribution

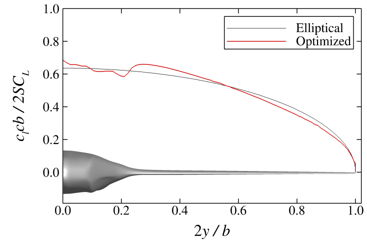

(b) Spanwise lift distribution

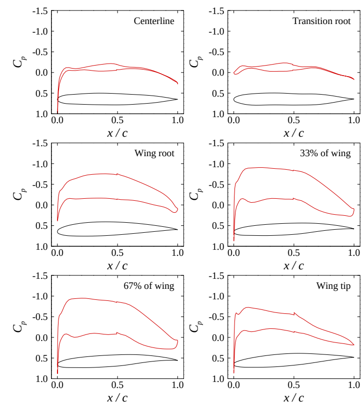

(c) Sectional pressure distributions

Figure 13: Solution information for the optimized LFC160-1 design.

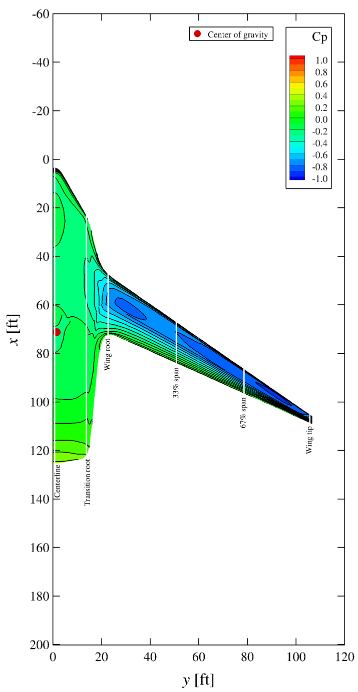

(a) Surface pressure distribution

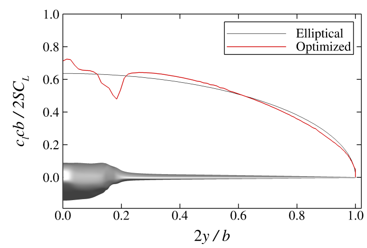

(b) Spanwise lift distribution

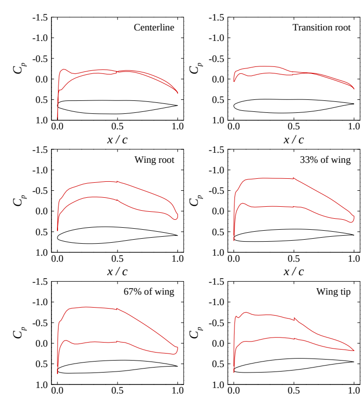

(c) Sectional pressure distributions

Figure 14: Solution information for the optimized LFC220-1 design.

Table 8: LFC performance at the start of cruise. Fuel-burn is that of the cruise segment, and is given relative to the optimized CTW in each class.

Design	Weight [lb]	S [ft^2]	C_L [–]	C_D [–]	L/D [–]	D/q_∞ [ft^2]	Drag [lb]	Relative fuel-burn [%]
LFC100-1	104,100	2,674	0.191	0.0080	24.0	21.3	4,338	−6.1
LFC160-1	177,700	3,457	0.246	0.0088	27.9	30.6	6,369	−9.7
LFC220-1	365,500	6,277	0.272	0.0090	30.3	56.4	12,063	–

Table 9: Optimized CTW performance at the start of cruise at their optimal altitude.

Design	Altitude [ft]	Weight [lb]	S [ft^2]	C_L [–]	C_D [–]	L/D [–]	D/q_∞ [ft^2]	Drag [lb]
CTW100-2	40,000	91,500	1,022	0.533	0.0265	20.1	27.1	4,552
CTW160-2	36,000	143,300	1,370	0.501	0.0247	20.3	33.8	7,059
CTW300-2	32,000	633,900	4,757	0.460	0.0189	24.3	90.0	26,086

of the LFC designs, the thickness-to-chord ratio at the centerline is quite reasonable at 9.6%, 9.7%, and 11.2%, smaller than that of the BWBs. While all designs are shock free, compared to the BWBs, the smaller thickness-to-chord ratio of the LFCs would aid in maintaining good off-design performance. For each class the wing volume and maximum thickness on the wing go to their lower bounds, as does the tip chord. All of the designs have a cruise angle-of-attack of between 2.5°and 3.0°. Note the sudden transition between the fuselage and wing for the LFC220-1 compared to the more gradual transition for the LFC100-1 and LFC160-1. This is a consequence of the cargo being located outboard of the passenger cabin for the LFC100 and LFC160 designs, while beneath the passenger cabin for the LFC220.

The fuselage for each LFC carries 32%, 28%, and 25% of the lift for the regional, narrow-body, and mid-size LFCs, respectively. This is in comparison to the BWBs which carry 31-43% of their lift on the center-body. Here, the center-body is taken to mean both the pressurized area and the transition region, i.e. the portion of lift not carried by the wings. While each LFC fuselage carries less lift than the corresponding BWB, it is a significantly larger fraction than the 12-13% carried by the CTW fuselages. For reference, the 'double-bubble' D8 configuration which features a lifting fuselage,[52] carries 19% of its lift on the fuselage. The LFC concept presented here shares features of both the BWB and D8 concepts. The LFC's fuselage carries more lift than that of the D8 but less than that of the BWB, and maintains the smooth transition between the fuselage and wing as present in the BWB concept.

V. Performance Studies

A. Operation at Optimal Altitude

As noted in Section III, the lower wing loading of the BWBs and LFCs implies a higher cruise altitude to attain the maximum lift-to-drag ratio. To determine the optimal altitude and the corresponding shape, the following process is followed. First, optimizations to maximize the lift-to-drag ratio are performed using the same variables, pitching moment constraint, and geometric constraints, as for the trim-constrained problems. This allows the optimizer to determine an optimal shape and an optimal lift coefficient. This results in lift coefficients higher than those for the trim-constrained cases. To satisfy $W = L = C_L S q_\infty$, this implies a higher cruise altitude for the BWBs and LFCs. However, since Reynolds number decreases with altitude, this would result in an increase in friction drag such that the resulting design would no longer be optimal. To address this, starting from the lift-to-drag ratio maximized result, trim-constrained drag minimization is performed at the altitude suggested by the lift-to-drag ratio maximization and at decrements of 2,000 ft with the target lift coefficient and Reynolds number adjusted accordingly. The altitude and design that provides the maximum lift-to-drag ratio from these optimizations is taken as the optimum and presented below. This procedure is performed for all of the CTWs, BWBs, and LFCs. This study is based upon aerodynamic performance considerations only and does not take into account the effects of altitude on engine performance,

Table 10: Optimized BWB performance at the start of cruise at their optimal altitude. Fuel-burn is that of the cruise segment, and is given relative to the optimized CTW in each class.

Design	Altitude [ft]	Weight [lb]	S [ft^2]	C_L [–]	C_D [–]	L/D [–]	D/q_∞ [ft^2]	Drag [lb]	Relative fuel-burn [%]
BWB100-2	46,000	106,600	2,972	0.284	0.0115	24.8	34.1	4,298	−5.5
BWB160-2	44,000	185,300	4,346	0.301	0.0109	27.6	47.4	6,714	−5.0
BWB220-2	40,000	355,400	6,629	0.304	0.0104	29.1	69.2	12,213	–
BWB300-2	34,000	700,500	9,356	0.288	0.0096	30.0	89.9	23,350	−9.5

Table 11: Optimized LFC performance at the start of cruise at their optimal altitude. Fuel-burn is that of the cruise segment, and is given relative to the optimized CTW in each class.

Design	Altitude [ft]	Weight [lb]	S [ft^2]	C_L [–]	C_D [–]	L/D [–]	D/q_∞ [ft^2]	Drag [lb]	Relative fuel-burn [%]
LFC100-2	44,000	104,100	2,803	0.267	0.0107	24.9	30.1	4,181	−8.2
LFC160-2	40,000	177,700	3,616	0.286	0.0102	28.0	37.0	6,346	−10.3
LFC220-2	36,000	365,500	6,277	0.272	0.0090	30.3	56.4	12,063	–

buffet, or operational considerations. At the crest of the L/D-vs-C_L curve, changes in L/D with C_L can be relatively small. Thus, while the altitudes determined correspond to conditions closest to optimum, deviations in altitude can be permitted with only small reductions in the lift-to-drag ratio. The designs at their optimal altitudes are indicated by the suffix '-2'.

The performance at optimal altitude for the CTWs is shown in Table 9. The regional, narrow-body, and mid-size CTWs optimally cruise at 40,000, 36,000, and 32,000 ft, respectively. For the CTW100, the increase in cruise altitude of 4,000 ft corresponds to a 1.5% increase in L/D. The narrow-body CTW160-2's optimal altitude is 36,000 ft, the same as for the original studies. Finally, the CTW300-2 has an optimal altitude of 32,000 ft, which yields a lift-to-drag ratio increase of almost 4% relative to the CTW300-1 design at 36,000 ft.

Due to their low wing loading, all of the BWBs, except for the BWB300, have an optimal altitude greater than the original 36,000 ft, as shown in Table 10. The change in altitude for the smaller classes is substantial, at up to 10,000 ft for the regional-class BWB, which gives up to almost an 8% increase in the lift-to-drag ratio. While a substantial performance improvement is achieved just by cruising at a higher altitude, the accompanying considerations such as engine size, buffet, and the requirement to climb to such a high altitude for a short range mission, may make such an altitude impractical. As expected, for each class, the BWBs cruise higher than their CTW counterpart. The resulting shapes are similar to those shown in Sections III and IV, but the wing area has been increased for the BWBs cruising at the higher altitudes.

Due to their slightly higher wing loading than the BWBs, the change in altitude for the LFCs is less dramatic, with a correspondingly smaller change in the lift-to-drag ratio. The optimal altitude of the LFC220-2 remains the same, at 36,000 ft, while the change in the lift-to-drag ratio for the LFC160-2 is negligible, and that of the LFC100-2 is less than 4%. The performance is summarized in Table 11. As with the BWBs, the wing area increases relative to the designs optimized at 36,000 ft.

B. Performance Comparison of the Three Concepts

This section examines the relative performance of the three concepts. The lift-to-drag ratio and relative cruise fuel-burn for each class are shown in Figure 15 for the results at 36,000 ft, and in Figure 16 at each design's optimal altitude. Fuel-burn is given relative to the optimized CTW in each class.

The aerodynamic efficiency, i.e. the lift-to-drag ratio, of the BWBs and LFCs is greater than that of the CTWs across all classes. For both the BWBs and LFCs there is a much more rapid increase in the lift-to-drag ratio between the regional and narrow-body classes than for the CTWs. Across all classes, the LFC concepts have lift-to-drag ratios still higher than the BWBs. When permitted to operate at their optimal altitude, the increase in the aerodynamic efficiency is greatest for the smaller classes of BWBs and LFCs.

While all of the BWBs exhibit higher aerodynamic efficiency than the CTWs, for each class, the BWBs

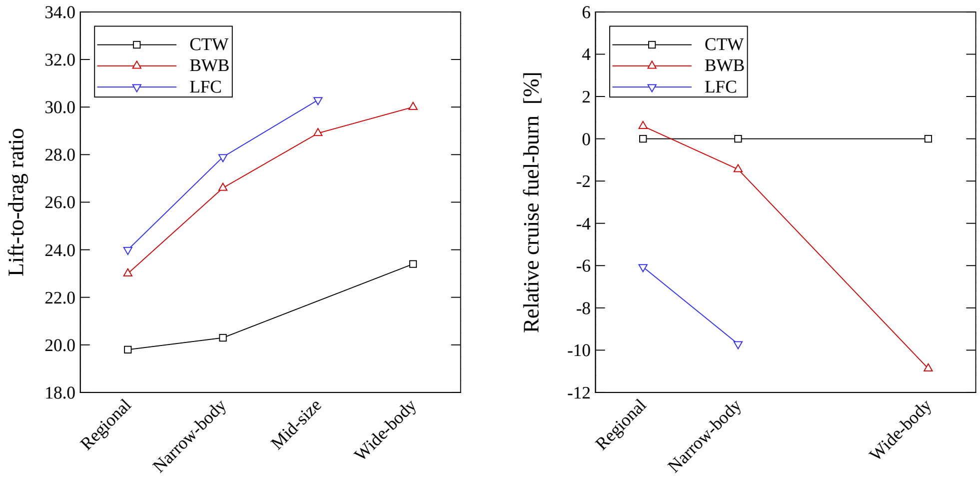

(a) Lift-to-drag ratio

(b) Relative cruise fuel-burn

Figure 15: The lift-to-drag ratio and relative cruise fuel-burn across all aircraft classes at 36,000 ft. Fuel-burn is given relative to that of the CTW for each class at 36,000 ft.

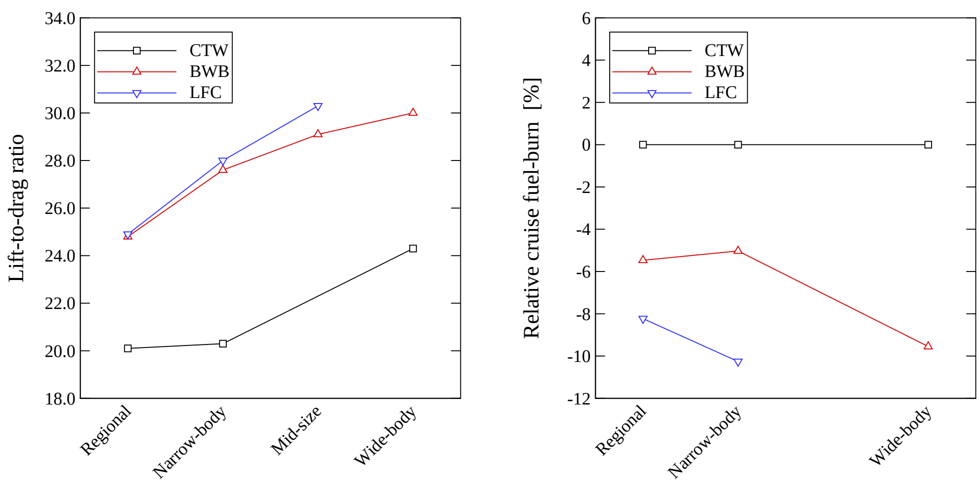

(a) Lift-to-drag ratio

(b) Relative cruise fuel-burn

Figure 16: The lift-to-drag ratio and relative cruise fuel-burn across all aircraft classes at their optimal altitude. Fuel-burn is given relative to that of the CTW for each class at its optimal altitude.

are heavier than their CTW counterpart, such that not all of the aerodynamic efficiency benefits are realized in terms of drag, and hence fuel-burn, reductions. The regional and narrow-body-class BWBs exhibit little fuel-burn reduction relative to the CTWs, as shown in Figure 15(b). Allowing the designs to operate at their optimal altitude increases the lift-to-drag ratio enough that the smaller BWBs can produce a fuel-burn reduction for the small classes of almost 6%; see Figure 16(b). The wide-body-class BWB burns up to almost 11% less fuel than the optimized CTW.

The combination of the LFC's lower weight and higher lift-to-drag ratio allows this concept to achieve a fuel-burn reduction relative to the CTWs of 6-10% for the regional and narrow-body classes. This benefit increases to over 8-10% if the designs cruise at their optimal altitude. The relative fuel-burn performance of the mid-size BWB and LFC is not given in Figures 15 and 16 since there is no mid-size CTW reference aircraft. The LFC220-1 has 2.1% lower fuel-burn than the BWB220-1 at 36,000 ft, and the LFC220-2 has 1.1% lower fuel-burn than the BWB220-2. The performance difference between the LFC and BWB concepts is smaller in this class than for the regional and narrow-body classes since the two concepts are approaching each other at this larger size.

The improved performance of the LFCs is largely a consequence of their lower wetted areas. While the regional and narrow-body-class BWBs have 14-18% higher wetted area than the CTWs, and the LFCs still have higher wetted area than the CTWs, the difference is reduced to 10% and 1% for the regional and narrow-body-class LFCs, respectively. The increased wetted area is, however, accompanied by a larger span, such that the wetted aspect ratio of the LFCs is 43% and 60% higher than the CTW100-1 and CTW160-1, respectively.

VI. Conclusions

The aerodynamic performance of BWB aircraft for a range of classes, from regional jets through wide-bodies, was investigated and compared with equivalent conventional tube-and-wing designs. In agreement with the literature, the aerodynamic performance of 'classically' shaped BWBs scales with increasing aircraft size, with the BWB concept offering a marginal drag and fuel-burn benefit for regional and narrow-body class aircraft, and up to a 13.8% drag, and a 10.9% fuel-burn reduction relative to the CTW for the wide-body class.

High-fidelity RANS-based exploratory aerodynamic shape optimization was then used to investigate BWB shapes that offer maximum aerodynamic efficiency. For all but the largest aircraft studied, the shape for the maximum lift-to-drag ratio has a more slender lifting fuselage and distinct wing than is seen in the classical design. The extent of these features forms a continuum, where, for the larger aircraft, the classical BWB concept is optimal. This configuration allows for reduced wetted area. Based on these results, lifting-fuselage configurations (LFCs) were created and optimized aerodynamically. The optimized LFCs produce higher lift-to-drag ratios than the BWB designs across all aircraft sizes. Combined with lower weight, this results in reduced drag and fuel-burn relative to both the BWB and CTW designs for all classes. While the spanwise extent of the fuselage is reduced for the LFCs relative to the BWBs, they still carry a substantial portion of lift, 25-32%, compared to the 31-43% of the BWBs, and 12-13% of the CTWs.

All of the above results were obtained at 36,000 ft. Additional optimizations were performed to determine the aerodynamically optimal cruise altitude of all the concepts. To attain their maximum aerodynamic efficiency, both the BWB and LFC concepts must cruise higher than the comparable CTWs. The change in cruise altitude is greatest for the BWBs, such that all of the BWBs now exhibit lower fuel-burn than the CTWs. While there was little fuel-burn benefit for the regional and narrow-body-class BWBs at 36,000 ft, they burn up to 5.5% less fuel in cruise when operated at their optimal altitude. The fuel-burn benefit of the LFCs increases to 8.2% and 10.3% for the regional-class and narrow-body classes, respectively. The high altitude required to achieve the maximum lift-to-drag ratio for the BWBs and LFCs may be impractical, particularly for the regional-class, in which case, the LFC becomes the only concept to offer lower fuel-burn than the CTWs in this class.

This paper has resulted in the initial development of a lifting-fuselage configuration which offers improved aerodynamic performance relative to both BWB and conventional designs. It is particularly well suited to smaller aircraft classes where the BWB concept provides little to no benefit. Reducing structural weight of this concept, which, like the BWB, may require a non-cylindrical pressure vessel, will be critical to allow for the realization of the full aerodynamic efficiency of this concept as reduced fuel-burn. Recent work[53] suggests that the weight of the non-cylindrical pressure vessel could likely be reduced through advanced structural design. This would allow a greater portion of the aerodynamic efficiency benefit of the unconventional concepts to be realized as reductions in fuel-burn. Other challenges of the LFC concept, most of which are also associated with the BWB concept, such as stability and control, engine installation, passenger acceptance, etc., will have to be addressed.

Acknowledgments

Financial support is provided in part by the Natural Sciences and Engineering Research Council of Canada and the University of Toronto. Computations were performed on the General Purpose Cluster supercomputer at the SciNet HPC Consortium. SciNet is funded by: the Canada Foundation for Innovation under the auspices of Compute Canada; the Government of Ontario; Ontario Research Fund - Research Excellence; and the University of Toronto.

References

[1]Liebeck, R. H., "Design of the Blended Wing Body Subsonic Transport," *Journal of Aircraft*, Vol. 41, No. 1, 2004, pp. 10–25.

[2]Li, V. and Velicki, A., "Advanced PRSEUS Structural Concept Design and Optimization," *12th AIAA/ISSMO Multidisciplinary Analysis and Optimization Conference*, No. AIAA-2008-5840, Victoria, BC, September 2008.

[3]Mukhopadhyay, V., Sobieszczanski-Sobieski, J., Kosaka, I., Quinn, G., and Vanderplaats, G. N., "Analysis, Design, and Optimization of Noncylindrical Fuselage for Blended-Wing-Body Vehicle," *Journal of Aircraft*, Vol. 41, No. 4, 2004, pp. 925–930.

[4]Hansen, L. U., Heinze, W., and Horst, P., "Blended Wing Body Structures in Multidisciplinary Pre-Design," *Structural and Multidisciplinary Optimization*, Vol. 38, No. 1, 2008, pp. 93–106.

[5]Vicroy, D. D., "Blended-Wing-Body Low-Speed Flight Dynamics: Summary of Ground Tests and Sample Results," *47th AIAA Aerospace Sciences Meeting and Exhibit*, No. AIAA-2009-0933, Orlando, FL, January 2009.

[6]Voskuijl, M., La Rocca, G., and Dircken, F., "Controllability of Blended Wing Body Aircraft," *26th International Congress of the Aeronautical Sciences*, Anchorage, AL, September 2008.

[7]Nickol, C. L., "Hybrid Wing Body Configuration Scaling Study," *50th AIAA Aerospace Sciences Meeting and Exhibit*, No. AIAA-2012-0337, Nashville, TN, January 2012.

[8]Wakayama, S., "Blended-Wing-Body Optimization Problem Setup," *8th AIAA/USAF/NASA/ISSMO Symposium on Multidisciplinary Analysis and Optimization*, No. AIAA-2000-4740, Long Beach, CA, September 2000.

[9]Hileman, J. I., Spakovszky, Z. S., Drela, M., and Sargeant, M. A., "Airframe Design for "Silent Aircraft"," *45th AIAA Aerospace Sciences Meeting and Exhibit*, No. AIAA-2007-0453, Reno, NV, January 2007.

[10]Hileman, J. I., Spakovszky, Z. S., Drela, M., Sargeant, M. A., and Jones, A., "Airframe Design for Silent Fuel-Efficient Aircraft," *Journal of Aircraft*, Vol. 47, No. 3, 2010, pp. 956–969.

[11]Morris, A. J., "MOB: A European Distributed Multi-Disciplinary Design and Optimisation Project," *9th AIAA/ISSMO Symposium on Multidisciplinary Analysis and Optimization*, No. AIAA-2002-5444, Atlanta, GA, September 2002.

[12]Méheut, M., Grenon, R., Carrier, G., Defos, M., and Duffau, M., "Aerodynamic Design of Transonic Flying Wing Configurations," *CEAS Katnet II Conference on Key Aerodynamic Technologies*, Breme, Germany, May 2009.

[13]Peigin, S. and Epstein, B., "Computational Fluid Dynamics Driven Optimization of Blended Wing Body Aircraft," *AIAA Journal*, Vol. 44, No. 11, 2006, pp. 2736–2745.

[14]Qin, N., Vavalle, A., Le Moigne, A., Laban, M., Hackett, K., and Weinerfelt, P., "Aerodynamic Considerations of Blended Wing Body Aircraft," *Progress in Aerospace Sciences*, Vol. 40, No. 6, 2004, pp. 321–343.

[15]Le Moigne, A. and Qin, N., "Aerofoil Profile and Sweep Optimisation for a Blended Wing-Body Aircraft Using A Discrete Adjoint Method," *The Aeronautical Journal*, Vol. 110, No. 1111, 2006, pp. 589–604.

[16]Lyu, Z. and Martins, J. R. R. A., "Aerodynamic Shape Optimization of a Blended-Wing-Body Aircraft," *51st AIAA Aerospace Sciences Meeting*, No. AIAA-2013-0283, Grapevine, TX, January 2013.

[17]Lyu, Z. and Martins, J. R. R. A., "Aerodynamic Shape Optimization Studies of a Blended-Wing-Body Aircraft," *Journal of Aircraft*, Vol. 51, No. 5, 2014, pp. 1604–1617.

[18]Kuntawala, N. B., Hicken, J. E., and Zingg, D. W., "Preliminary Aerodynamic Shape Optimization of a Blended-Wing-Body Aircraft Configuration," *49th AIAA Aerospace Sciences Meeting*, No. AIAA-2011-0642, Orlando, FL, January 2011.

[19]Reist, T. A. and Zingg, D. W., "Aerodynamic Shape Optimization of a Blended-Wing-Body Regional Transport for a Short Range Mission," *31st AIAA Applied Aerodynamics Conference*, No. AIAA-2013-2414, San Diego, CA, June 2013.

[20]Reist, T. A. and Zingg, D. W., "High-Fidelity Aerodynamic Shape Optimization of Regional-Class Blended Wing-Body and Lifting-Fuselage Aircraft," *Journal of Aircraft*, (Submitted).

[21]Reist, T. A. and Zingg, D. W., "Optimization of the Aerodynamic Performance of Regional and Wide-Body-Class Blended Wing-Body Aircraft," *33rd AIAA Applied Aerodynamics Conference*, No. AIAA-2015-3239, Dallas, TX, June 2015.

[22]Hicken, J. E. and Zingg, D. W., "A Parallel Newton-Krylov Solver for the Euler Equations Discretized Using Simultaneous Approximation Terms," *AIAA Journal*, Vol. 46, No. 11, 2008, pp. 2773–2786.

[23]Osusky, M. and Zingg, D. W., "A Parallel Newton-Krylov-Schur Flow Solver for the Navier-Stokes Equations Discretized Using Summation-By-Parts Operators," *AIAA Journal*, Vol. 51, No. 12, 2013, pp. 2833–2851.

[24]Hicken, J. E. and Zingg, D. W., "Aerodynamic Optimization Algorithm with Integrated Geometry Parameterization and Mesh Movement," *AIAA Journal*, Vol. 48, No. 2, 2010, pp. 401–413.

[25]Gill, P. E., Murray, W., and Saunders, M. A., "SNOPT: An SQP Algorithm for Large-Scale Constrained Optimization," *Society for Industrial Applied Mathematics Review*, Vol. 47, No. 1, 2005, pp. 99–131.

[26]Osusky, L., Buckley, H., Reist, T., and Zingg, D. W., "Drag Minimization Based on the Navier-Stokes Equations Using a Newton-Krylov Approach," *AIAA Journal*, Vol. 53, No. 6, 2015, pp. 1555–1577.

[27]Gagnon, H. and Zingg, D. W., "Two-Level Free-Form and Axial Deformation for Exploratory Aerodynamic Shape Optimization," *AIAA Journal*, Vol. 53, No. 7, 2015, pp. 2015–2026.

[28]Zingg, D. W., Nemec, M., and Pulliam, T. H., "A Comparative Evaluation of Genetic and Gradient-Based Algorithms Applied to Aerodynamic Optimization," *European Journal of Computational Mechanics*, Vol. 17, No. 1, 2008, pp. 103–126.

[29]Chernukhin, O. and Zingg, D. W., "Multimodality and Global Optimization in Aerodynamic Design," *AIAA Journal*, Vol. 51, No. 6, 2013, pp. 1342–1354.

[30]Hicken, J. E. and Zingg, D. W., "A Simplified and Flexible Variant of GCROT for Solving Nonsymmetric Linear Systems," *SIAM Journal of Scientific Computing*, Vol. 32, No. 3, 2010, pp. 1672–1694.

[31]Hicken, J. E. and Zingg, D. W., "Induced Drag Minimization of Nonplanar Geometries Based on the Euler Equations," *AIAA Journal*, Vol. 48, No. 11, 2010, pp. 2564–2575.

[32]Leung, T. M. and Zingg, D. W., "Aerodynamic Shape Optimization of Wings Using a Parallel Newton-Krylov Approach," *AIAA Journal*, Vol. 50, No. 3, 2012, pp. 540–550.

[33]Leung, T. M. and Zingg, D. W., "Design of Low-Sweep Wings for Maximum Range," *29th AIAA Applied Aerodynamics Conference*, No. AIAA-2011-3178, Honolulu, HI, June 2011.

[34]Gagnon, H. and Zingg, D. W., "Geometry Generation of Complex Unconventional Aircraft with Application to High-Fidelity Aerodynamic Shape Optimization," *21st AIAA Computational Fluid Dynamics Conference*, No. AIAA-2013-2850, San Diego, CA, June 2013.

[35]Gagnon, H. and Zingg, D. W., "High-Fidelity Aerodynamic Shape Optimization of Unconventional Aircraft through Axial Deformation," *52nd Aerospace Sciences Meeting*, No. AIAA-2014-0908, National Harbor, MD, January 2014.

[36]Gagnon, H. and Zingg, D. W., "Aerodynamic Optimization Trade Study of a Box-Wing Aircraft Configuration," *Journal of Aircraft*, 2015. doi:10.2514/1.C033592, (Accepted August 2015).

[37]Gagnon, H. and Zingg, D. W., "Euler-Equation-Based Drag Minimization of Unconventional Aircraft Configurations," *Journal of Aircraft*, 2015, (Accepted December 2015).

[38]Zhang, Z. J., Khosravi, S., and Zingg, D. W., "High-Fidelity Aerostructural Optimization with Integrated Geometry Parameterization and Mesh Movement," *56th AIAA/ASCE/AHS/ASC Structures, Structural Dynamics, and Materials Conference*, No. AIAA-2015-1132, Kissimmee, FL, January 2015.

[39]Khosravi, S. and Zingg, D. W., "A Numerical Optimization Study on Winglets," *15th AIAA/ISSMO Multidisciplinary Analysis and Optimization Conference*, No. AIAA-2014-2173, Atlanta, GA, June 2014.

[40]Embraer Commercial Aircraft, *Embraer 190 Airport Planning Manual*, 2005, (Revision 10 - 18 February 2013).

[41]Boeing Commercial Airplanes, *737 Airplane Characteristics for Airport Planning*, 2013.

[42]Boeing Commercial Airplanes, *767 Airplane Characteristics for Airport Planning*, 2005.

[43]Boeing Commercial Airplanes, *777-200LR/-300ER/-Freighter Airplane Characteristics for Airport Planning*, 2009.

[44]Torenbeek, E., *Synthesis of Subsonic Airplane Design*, Delft University, 1976.

[45]"Aircraft Design: Synthesis and Analysis," http://adg.stanford.edu/aa241/AircraftDesign.html, December 2014.

[46]Raymer, D. P., *Aircraft Design: A Conceptual Approach*, American Institute of Aeronautics and Astronautics, 5th ed., 2012.

[47]Bradley, K. R., "A Sizing Methodology for the Conceptual Design of Blended-Wing-Body Transports," Tech. Rep. NASA/CR-2004-213016, NASA/Langley Research Center: Joint Institute for Advancement of Flight Sciences, 2004.

[48]Buckley, H. P. and Zingg, D. W., "An Approach to Aerodynamic Design Through Numerical Optimization," *AIAA Journal*, Vol. 51, No. 8, 2013, pp. 1972–1981.

[49]Qin, N., Vavelle, A., and Le Moigne, A., "Spanwise Lift Distribution for Blended Wing Body Aircraft," *Journal of Aircraft*, Vol. 42, No. 2, 2005, pp. 356–365.

[50]Sargeant, M. A., Hynes, T. P., Graham, W. R., Hileman, J. I., Drela, M., and Spakovszky, Z. S., "Stability of Hybrid-Wing-Body Aircraft with Centerbody Leading-Edge Carving," *Journal of Aircraft*, Vol. 47, No. 3, 2010, pp. 970–974.

[51]Mialon, B., Fol, T., and Bonnaud, C., "Aerodynamic Optimization of Subsonic Flying Wing Configurations," *20th AIAA Applied Aerodynamics Conference*, No. AIAA-2002-2931, St. Louis, MO, 2002.

[52]Drela, M., "Development of the D8 Transport Configuration," *29th AIAA Applied Aerodynamics Conference*, Honolulu, HI, June 2011.

[53]Mukhopadhyay, V. and Sorokach, M. R., "Composite Structure Modeling and Analysis of Advanced Aircraft Fuselage Concepts," *AIAA Modeling and Simulation Technologies Conference*, No. AIAA-2015-3096, Dallas, TX, 2015.